

ARTICLE

## SAR Change Detection Algorithm Combined with FFDNet Spatial Denoising

Yuqing Wu<sup>1</sup>, Qing Xu<sup>\*</sup>, Zheng Zhang, Jingzhen Ma, Tianming Zhao, Xinming Zhu

*Institute of Geospatial Information, Information Engineering University, Zhengzhou, Henan, 450001, China*

### ABSTRACT

**Objectives:** When detecting changes in synthetic aperture radar (SAR) images, the quality of the difference map has an important impact on the detection results, and the speckle noise in the image interferes with the extraction of change information. In order to improve the detection accuracy of SAR image change detection and improve the quality of the difference map, this paper proposes a method that combines the popular deep neural network with the clustering algorithm. **Methods:** Firstly, the SAR image with speckle noise was constructed, and the FFDNet architecture was used to retrain the SAR image, and the network parameters with better effect on speckle noise suppression were obtained. Then the log ratio operator is generated by using the reconstructed image output from the network. Finally, K-means and FCM clustering algorithms are used to analyze the difference images, and the binary map of change detection results is generated. **Results:** The experimental results have high detection accuracy on Bern and Sulzberger's real data, which proves the effectiveness of the method.

**Keywords:** SAR change detection; Image noise reduction; FFDNet; Difference diagram; Clustering algorithm

## 1. Introduction

Synthetic aperture radar (SAR) imagery has been widely utilized in various fields<sup>[1]</sup>. It can be applied by public institutions for urban planning purposes, while also providing valuable assistance to military

personnel in decision-making processes<sup>[2]</sup>. Various surface features have a significant impact on SAR imaging<sup>[3]</sup>. Factors such as snow cover, topographic characteristics, and man-made structures need to be taken into account for accurate interpretation and analysis of SAR image data. For fields like environ-

#### \*CORRESPONDING AUTHOR:

Qing Xu, Institute of Geospatial Information, Information Engineering University, Zhengzhou, Henan, 450001, China; Email: xq2021ch@126.com

#### ARTICLE INFO

Received: 21 September 2023 | Revised: 20 October 2023 | Accepted: 26 October 2023 | Published Online: 10 November 2023

DOI: <https://doi.org/10.30564/jees.v5i2.5980>

#### CITATION

Wu, Y.Q., Xu, Q., Zhang, Zh., et al., 2023. SAR Change Detection Algorithm Combined with FFDNet Spatial Denoising. Journal of Environmental & Earth Sciences. 5(2): 88-101. DOI: <https://doi.org/10.30564/jees.v5i2.5980>

#### COPYRIGHT

Copyright © 2023 by the author(s). Published by Bilingual Publishing Group. This is an open access article under the Creative Commons Attribution-NonCommercial 4.0 International (CC BY-NC 4.0) License. (<https://creativecommons.org/licenses/by-nc/4.0/>).

mental monitoring, disaster assessment, and urban planning, SAR technology provides valuable and comprehensive information sources [4]. However, the multiplicative speckle noise in SAR imaging has caused practical difficulties in the interpretation of the targets shot in the image [5]. Because the speckle noise in SAR images has an important impact on the generation of change detection results, removing the speckle noise in the image has become an important way to improve the detection accuracy of SAR change detection.

For SAR image change detection, there are two main methods: direct classification and generation of difference image (DI) [2,6]. The first is to process the original input images respectively; the second is to first comprehensively consider the differences between the two-phase images and generate the difference image, and then use clustering and other methods to generate the binary image of the change detection results. In the method of generating the difference image, many scholars have improved the detection accuracy by improving the quality of the difference image and optimizing the clustering algorithm. Many scholars have made important contributions in removing speckle noise and integrating it into the clustering algorithm. K-means clustering is used to generate the detection binary image [7]. FCM (Fuzzy C-Means Clustering) is used to classify the different images into three categories, and then a neural network is used for classification [2]. Gong et al. [6] employed fusion to combine the mean ratio and logarithmic ratio difference graphs, and then used the improved fuzzy C-means algorithm for change detection, which not only improved the quality of the difference graphs, but also made contributions to improving subsequent clustering methods. Gao et al. [8] introduced the dual-tree complex wavelet transform into the convolutional neural network to classify changed and unchanged pixels, so as to reduce speckle noise in the image. Qu et al. [9] used the frequency domain information of the image to reduce speckle noise.

The main goal of change detection in SAR image analysis is to identify and analyze SAR images

captured at different time periods within the same region, particularly dual-phase images [9]. The primary task involves classifying individual pixels in the image as either altered or unaltered. Clustering algorithms are commonly utilized for this purpose, as they effectively classify sample data to detect changes. Several researchers have improved clustering methods to enhance detection accuracy. Shang et al. [10] introduced a mean classification technique followed by fuzzy clustering, while Gao et al. [2] employed the FCM clustering algorithm initially to categorize pixel points into three groups and then used neural networks for generating results. Many scholars have also combined deep learning techniques with clustering algorithms, resulting in significant enhancements in detection accuracy. The above methods have greatly improved the detection accuracy of change detection by combining clustering and deep learning. However, whether feature extraction is performed through difference image fusion or convolutional network, the setting of difference image fusion coefficient weight and robust methods for speckle noise suppression are still worth exploring.

Therefore, before change detection, reducing the speckle noise of the image has become the main content of many scholars' research. Because the clustering algorithm is sensitive to noise [1,11], literature [12] first uses the PPB (the probabilistic-patch-based algorithm) filter to weaken noise before difference operator fusion. Tan et al. [13] proposed a new end-to-end self-supervised SAR denoising model: Enhanced Noise2Noise (EN2N) to solve the problem of detail loss caused by CNN. Zhang et al. [14] proposed FFDNet network architecture, which has excellent ability in image balance denoising and detail retention.

In order to improve the quality of difference maps, this paper proposes a two-phase SAR image change detection method based on FFDNet, which will use a deep neural network to denoise SAR images for change detection. Our contributions are mainly in two aspects:

(1) use the FFDNet model framework in a deep neural network to denoise difference maps and generate more universal difference images;

(2) combine traditional clustering with deep learning, use the network to minimize speckle noise and classify rapidly through clustering. By combining the advantages of the two methods, the performance of the algorithm is improved.

## 2. Experimental method

The method proposed in this paper is shown in **Figure 1**, which combines the network with the traditional clustering method, takes the two-phase image as the input of the FFDNet network, calculates the corresponding difference operator of the denoised image, and then makes the change detection result graph through clustering analysis. In this section, the difference operator, FFDNet and clustering method in the experiment are introduced.

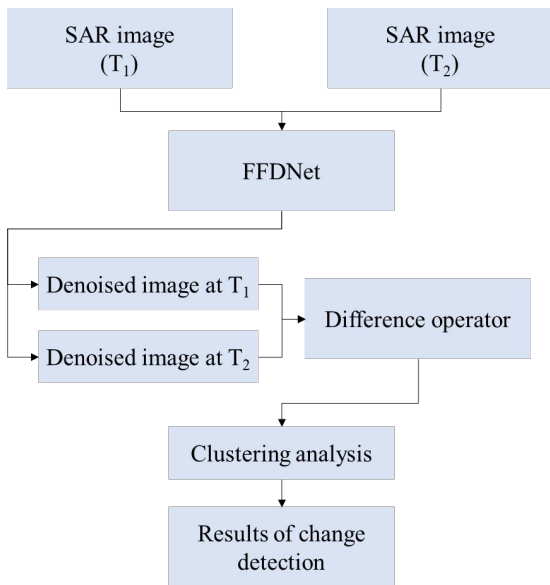


Figure 1. Method flow chart.

### 2.1 FFDNet denoising model

The main idea of the FFDNet-based image denoising method is to use the network to learn the noise in the original image, and then use the original image and the noise in the network to reduce the noise to achieve image denoising [15]. The existing CNN denoising tends to Gaussian noise, and has poor generalization ability for real noisy images with more complex noise [16]. In order to solve the problem of different noise levels, the topic of edge detection on SAR images has been extensively studied in the literature [17], providing valuable knowledge to improve our understanding and application of Synthetic Aperture Radar (SAR) technology. Kai et al. [14] used noise level map as input. The research findings [18] indicate that the use of ratio information is not suitable for edge detection. Nevertheless, incorporating various types of information through fusion techniques has been proven to greatly enhance the precision of detection, thereby enhancing its effectiveness.

FFDNet network uses Gaussian noise to model image noise, and has a weak effect on the removal of speckle noise in SAR images. Therefore, this paper uses speckle noise as a sample to re-train and design a noise model that conforms to SAR images. It is mainly composed of a convolution neural network, which can remove a wider range of noise when processing sampling operators. The experiment uses the speckle noise in the original real SAR image as input, and the network structure is shown in **Figure 2**.

The input  $Y$  consists of a reversible downsampling operator, which reshapes the input image into

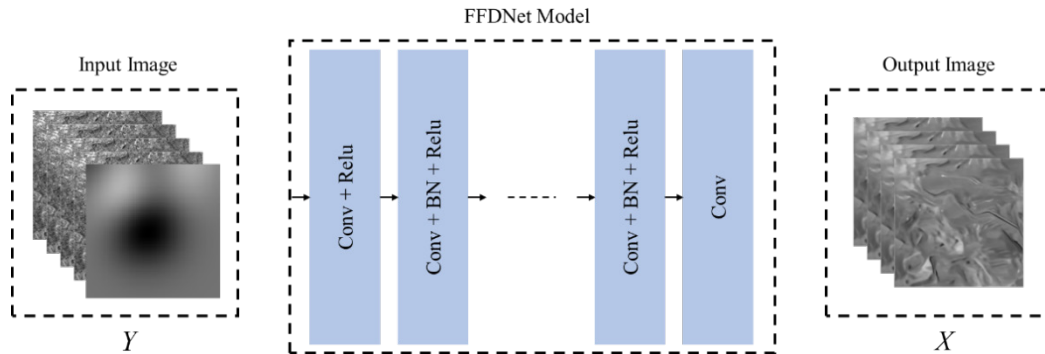


Figure 2. The architecture of the FFDNet for image denoising.

four downsampling images, and together with the noise level image, becomes the input of the convolution. The noise level image specifies a specific noise level for each pixel of the image, which is used to manage the trade-off between noise reduction and detail preservation in the case of spatially varying noise<sup>[16,19,20]</sup>.

The size of input image  $Y$  is defined as  $W \times H \times C$ , subimage after downsampling is  $\frac{W}{2} \times \frac{H}{2} \times 4C$ .  $Y$  represents the input image object,  $W$  denotes the pixel width of the image, and  $H$  represents the pixel height of the image.  $C$  is the number of channels of the image, and is 1 in the SAR denoising model. Subimage and noise level graphs are connected together as the tensor of  $\frac{W}{2} \times \frac{H}{2} \times (4C+1)$ , which is used as the data input of CNN.

CNN is composed of a series of  $3 \times 3$  convolution layers, the first convolution layer is “Conv + ReLU”, the middle 15 layers are “Conv + BN + ReLU”, and the last Conv layer is “CONV”. Fill the feature map with zero to ensure the constant size of the feature map.

The output end is four denoised sub-images, which are restored to the original image after reconstruction. According to the FFDNet<sup>[10]</sup> team, when SAR gray image noise reduction is used, the convolutional layer of gray image is set to 15 layers, the feature mapping channel of gray image is set to 64, and the downsampling factor is set to 2.

We normalized the SAR input image without introducing additional errors in the calculation and without changing the information storage of the im-

age itself, and compressed the original image to the range of 0 to 1 by using Equation (1).  $y_i$  represents the pixel value of the  $i$ -th pixel point corresponding to input image  $Y$ .  $\max(y)$  and  $\min(y)$  are respectively the maximum and minimum pixel values of the corresponding images. The denoising process is shown in **Figure 3**.

$$norm = \frac{y_i - \min(y)}{\max(y) - \min(y)} \quad (1)$$

In forward propagation, FFDNet uses residual learning to train a residual map, as shown in Equation (2):

$$R(y_i; \lambda) \approx y_i - x_i \quad (2)$$

$R(y_i; \lambda)$  is the noise image predicted by the network,  $\lambda$  is the network parameter used for training,  $y_i$  is the original noise input image, and  $x_i$  is the noise-free label graph.  $N$  represents the number of pixels in the image.  $\Delta x_i$  is the substitute quantity used for approximate calculations in the backpropagation, the mean square error is used as the loss function and quantified, as shown in Equation (3), and the adaptive moment estimation (Adam) algorithm is used to minimize the loss function.

$$\partial(\lambda) = \frac{1}{2N} \sum_{i=1}^N \|\Delta x_i - x_i\|^2 \quad (3)$$

$$\Delta x_i = y_i - R(y_i - x_i) \quad (4)$$

where  $N$  is the number of training samples.

After the network is trained on SAR images with speckle noise, the real dataset is sent to the trained FFDNet, and the new network parameters are used to weaken the noise in the image, and then the four sub-images that generate downsampling are restored to the original image.

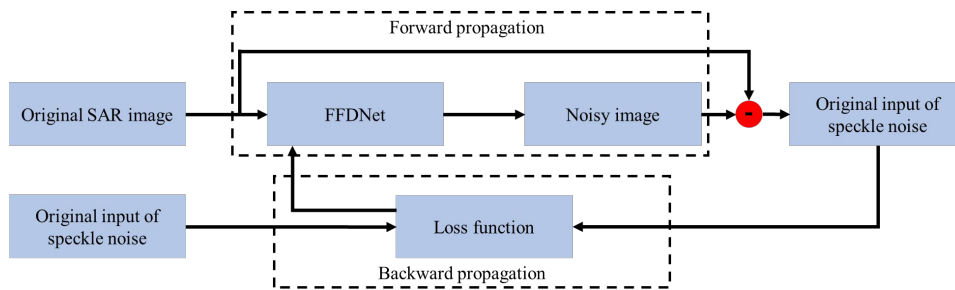


Figure 3. The architecture of the FFDNet for image denoising.

## 2.2 Logarithmic ratio operator and mean ratio operator

The generation effect of the difference map has a significant impact on the results of change detection. Essentially, the process of generating a difference map involves using specific algorithms to identify discrepancies between two images, initially highlighting areas that have changed in SAR images and providing a basis for subsequent analysis of difference maps to obtain change detection results. The logarithmic ratio operator incorporates logarithmic operations into the ratio method, effectively converting multiplicative noise models into additive noise models<sup>[12]</sup>. The logarithmic ratio method is widely employed for acquiring difference maps. However, this approach's drawback lies in its tendency to amplify pixel contraction characteristics through logarithmic operations, potentially resulting in inadequate preservation or even blurring of edge pixel details.

$$X_{LR} = \left| \log \frac{X_2}{X_1} \right| = |\log X_2 - \log X_1| \quad (5)$$

where  $X_2$  and  $X_1$  are input image information, the gray value in SAR image matrix is used in the calculation.

In order to avoid calculation error caused by zero pixel value in image  $X_{LR}$ , the calculated pixel value in Equation (5) is added by 1, and the logarithmic ratio operator is obtained by Equation (6).

$$D_L = \left| \log \frac{X_2 + 1}{X_1 + 1} \right| = |\log(X_2 + 1) - \log(X_1 + 1)| \quad (6)$$

$$X_{MR} = 1 - \min\left(\frac{X_2}{X_1}, \frac{X_1}{X_2}\right) \quad (7)$$

By using the neighborhood information of pixels, the mean ratio operator replaces the texture feature value or gray value of the corresponding pixel by averaging the neighborhood pixel, which can suppress the speckle of a single pixel shape. Goodman<sup>[13]</sup> has proved that the noise in SAR images is speckle noise. In this paper, a relatively ideal log-ratio and mean-ratio operator is used as the difference operator in the experiment.

## 2.3 Clustering algorithm

When analyzing the difference map and generating change detection results, there are threshold algorithms<sup>[23]</sup> and clustering algorithms<sup>[24]</sup>. Because the difference image cannot obtain an obvious boundary<sup>[25]</sup>, and the clustering algorithm does not need to establish a sample model, it is more flexible than the threshold method and has been widely used. As is widely known in the scientific literature<sup>[20]</sup> modeling for the difference image does not need any prior information about the data distribution of the difference image, and creates a feature space, and finally uses K-means clustering to generate detection results. Gong et al.<sup>[6]</sup> reconstructed the difference map, and then used the improved fuzzy local information C-means clustering to perform change detection. The following is an explanation of the clustering method used in this experiment. K-means algorithm is an early method used in clustering methods, which can quickly divide the data into multiple categories, and has a good clustering effect and universality. First,  $k$  initial clustering centers  $K_i$  are randomly selected from the data pixel points, and the sum of the squares of the distances between the pixel points and the selected clustering center points is taken as the objective function.

$$d = \sqrt{\sum_{j=1}^n \sum_{i=1}^m (x_i - K_i)^2} \quad (8)$$

where  $x_i$  is the traversal pixel,  $K_i$  is the cluster center initially randomly selected,  $n$  and  $m$  are the number of cluster centers and data dimension respectively. In this algorithm, Euclidean distance is used to calculate the distance from the cluster center, and each sample is classified into the class with the smallest distance. In change detection, each pixel in the SAR image is classified as changed or unchanged under the objective function, that is, the label is designated as one of  $\{0,1\}$ . Finally, the center of mass of each class is calculated, that is, the average distance between each pixel in the class and the center, and the new center point is adjusted according to this, until the cluster center is no longer changed.

FCM forms the classification of specified data

by optimizing the minimum objective function <sup>[26]</sup>, which is an improvement of K-means method and plays an important role in the field of data processing and analysis <sup>[27]</sup>. In change detection, the method calculates the membership degree between each pixel and the cluster center, and makes the objective function obtain the minimum value, so that all pixels can be classified. It is realized in the process of iteratively calculating membership degree  $u_{ij}$  and cluster center  $v_i$ .

Its objective function is:

$$J = \sum_{i=1}^c \sum_{j=1}^n u_{ij}^m d_{ij}^2 \quad (9)$$

where  $c$  is the specified number of categories,  $c = 2$  in the change detection experiment,  $n$  represents the number of pixels in the image, and  $u_{ij}$  represents the membership degree of the  $j$ -th pixel in the image belonging to the  $i$  cluster center.  $u_{ij}$  must satisfy the following two constraints.

$$\begin{cases} \sum_{i=1}^c u_{ij} = 1 \\ 0 \leq u_{ij} \leq 1 \end{cases} \quad (10)$$

$m$  is the fuzzy weight index, and different fuzzy weight indices have an impact on the clustering results and the time complexity of the algorithm. The value of this parameter is usually [1.5, 2.5]. Pal et al. considered  $m = 2$  to be the best through experimental verification <sup>[23]</sup>, and we also adopted this parameter in the experiment.  $d_{ij}$  is the distance between the  $j$ -th pixel point and the  $i$ -th cluster center point, which is consistent with the K-means clustering idea. Euclidean distance, which is simpler to calculate in two-dimensional data, is used for distance calculation.

$$d_{ij}^2 = \|x_j - v_i\|^2 \quad (11)$$

$x_j$  is the vector representation of the  $j$ -th sample point in the two-dimensional image, and  $v_i$  is the cluster center of the  $i$  class.

The iterative calculation formula of membership degree and cluster center is as follows:

$$u_{ij} = \left[ \sum_{k=0}^c \frac{d_{ij}^2}{d_{kj}^2} \right]^{-1} \quad (12)$$

$$v_i = \frac{\sum_{j=1}^n u_{ij}^m x_j}{\sum_{j=1}^n u_{ij}^m} \quad (13)$$

$U = [u_{ij}]$  is a matrix of  $c \times n$  size composed of membership degree,  $V = [v_i]$  is a matrix of  $n \times c$  size composed of cluster center, and  $n$  is the total number of pixels used for the classification of images. In this paper, cluster classification is carried out for all pixels in well-registered images.

## 2.4 Evaluation

The quantitative analysis of change detection results is set as follows:

PSNR (Peak Signal-to-Noise Ratio) is used to measure the difference between two images. This method is used to calculate the degree of difference between different difference graphs. The minimum value of PSNR is 0, and the larger the PSNR, the smaller the difference between the two images. The minimum value of SSIM <sup>[24]</sup> (structural similarity index) SSIM is 0 and the maximum value is 1. The larger the SSIM, the more similar the two images are.

FN (False Negatives): The number of changed pixels classified as non-changed pixels; FP (False Positives): Number of pixels that do not change. Total errors OE (Overall errors): Sum of missed FN and false alarms FP; PCC (Percentage Correct Classification): The ratio of the number of correct detections to the total pixels; Kappa coefficient <sup>[25]</sup> takes into account both correctly detected pixels and incorrectly detected pixels.

In the calculation of PCC and Kappa coefficient, two other indicators should be used: True Positive (TP): Change pixels are classified as the number of changed pixels; True Negative (TN): The number of non-changing pixels classified as non-changing pixels.

$$PCC = \frac{Num - OE}{Num} \quad (14)$$

$$\left\{ \begin{aligned} Kappa &= \frac{PCC - P}{1 - P} \\ P &= \frac{(TP + FN) \times (TP + FP)}{Num} \times \frac{(TN + FP) \times (TN + FN)}{Num} \end{aligned} \right. \quad (15)$$

Num can be represented as  $Num = TP + FP + FN + TN$ , which is the total number of image pixels; The closer the Kappa coefficient is to 1, the better the detection effect is.

In this paper, PSNR and SSIM were used to evaluate the similarity measure of the difference graph, and PCC and Kappa were used to compare the change detection result graph with the reference graph.

### 3. Experimental results and analysis

#### 3.1 Research data and experimental scheme

The interaction between radar waves and the Earth’s surface, as observed through Synthetic Aperture Radar (SAR) imaging technology, is significantly influenced by the moisture content of the soil. The dielectric constant of wet soil is higher compared to dry soil, resulting in increased attenuation of microwave signals emitted by SAR sensors at specific frequencies and subsequently reducing the depth of penetration. At the same time, when SAR sensors are used for observation, the snow-covered surface shows distinct characteristics. The dielectric properties of snow differ from those of other materials found on land, resulting in changes in the levels of backscattering energy detected by SAR systems. Due to the fine-scale roughness of snow, freshly fallen snow typically has increased reflectivity. However, on a larger scale, fresh snow exhibits reduced reflectivity

because of volume scattering effects caused by ice crystals within the layer of snow.

To validate the practicality of the experiment under the aforementioned circumstances, two distinct sets of actual data were chosen for comparative analysis. The reference figure of the research area and changes is shown in **Figure 4**. The first set of experimental data size  $301 \times 301$ , SAR images taken by the European Remote Sensing 2 satellite of the Swiss capital Bern city (Bern). **Figures 4a and 4b** show the flood situation near the outskirts of Bern, the capital of Switzerland, taken in April 1999 and May 1999 respectively. **Figure 4c** is the reference map of changes.

The second group of experimental data,  $256 \times 256$ , was captured by the Envisat satellite. As shown in **Figure 5**, a and b show the process of ice rupture on March 11, 2011 and March 16, 2011, respectively. The changes were mainly caused by the bending and breaking of the ice shelf due to huge sea waves<sup>[8]</sup>, and **Figure 5c** is the reference diagram of the changes.

In order to prove the effectiveness of the change detection algorithm combined with the FFDNet denoising model, experiments were carried out on the above two real data. Firstly, the FFDNet model is used to pre-process the image denoising, and the globally optimized high-quality difference map is constructed. Secondly, the log-ratio difference operator is constructed, and the performance of the mean-ratio operator in the experimental scheme is compared in the follow-up experiment. Finally, the difference map is classified and the final change detection result map is generated. The experimental

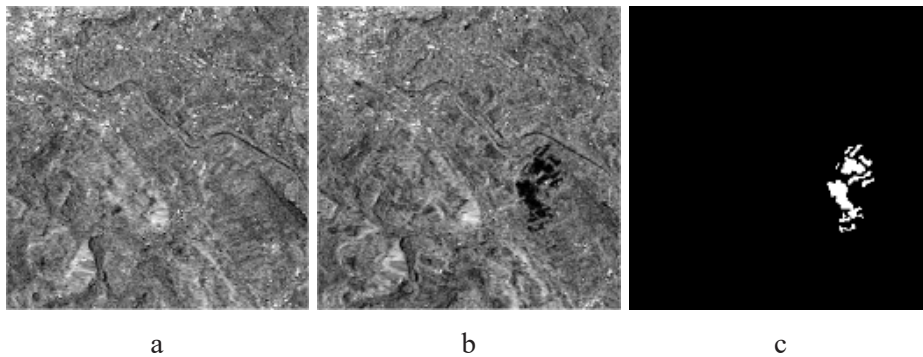


Figure 4. SAR image of Bern area.

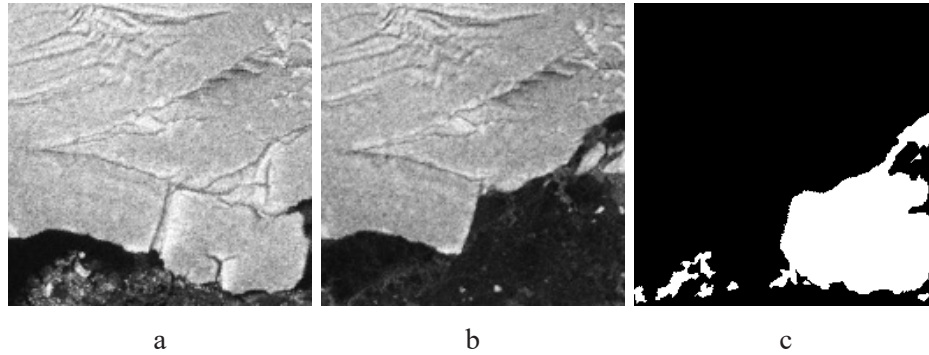


Figure 5. SAR image of Sulzberger area.

environment was Inter Core i7-1160G7, a computer with 16G memory, and the experimental programming language was Python.

### 3.2 Difference operator denoising results

Figures 6 and 7 are the results of de-noising through the FFDNet network, which inhibits speckle noise and makes the overall image smoother. Areas of change that are not caused by floods are more significant in the Bern dataset, and noise levels in the exposed sea surface in the Sulzberger dataset are reduced.

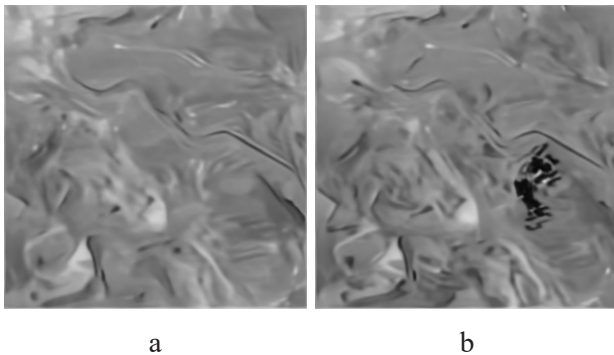


Figure 6. Bern region denoised image.

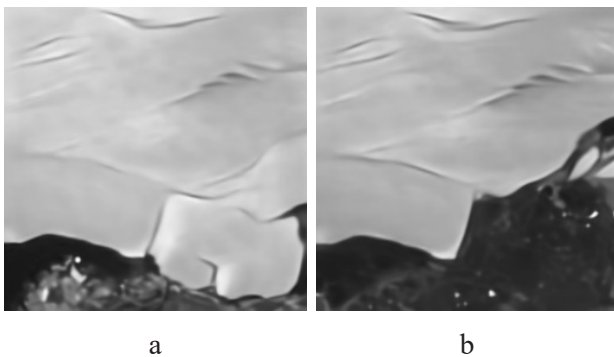


Figure 7. Sulzberger region denoised image.

The difference operator is the earliest method applied to change detection and the simplest one. In this section, to verify the validity of the proposed difference operator, the difference operator is used as the basic operator of the two-phase image, and is compared with the logarithm ratio, the mean value operator and the operator after FFDNet denoising, and the PSNR and SSIM values of the difference operator are calculated. The results are shown in Figure 8. The model proposed in this paper takes the average value of the whole image, and some details are lost in the flat region, resulting in a certain degree of blur, but the speckle noise is obviously suppressed.

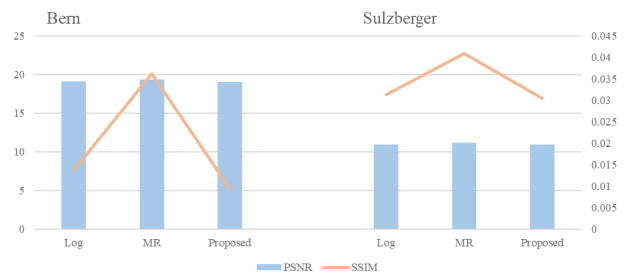


Figure 8. Evaluation index of different difference operators in Bern and Sulzberger region.

### 3.3 Change detection results and analysis

The experimental results of Bern dataset are shown in Figure 9 and Table 1. Classical K-means clustering [25] and FCM clustering [11] algorithms generate more discrete noise points in Bern. As the basic clustering method does not consider other information of the data in the spatial space, it is more

sensitive to image noise. As can be seen from the figure, the original clustering method generates more discrete isolated points, and many missing units are also generated in the flood coverage area. Through feature dimension extraction, PCAKM<sup>[7]</sup> algorithm significantly reduces noise points, and makes image edges smoother, edges of changing subjects smoother, and Outlines clearer. PCANet<sup>[2]</sup> has an obvious suppression effect on speckle noise after pre-classification, but the main content is also compressed to a certain extent, and part of the change information is lost, so the effect on Kappa index is low.

Sulzberger datasets are shown in Figure 10 and Table 2 in several experimental results. The classical K-means clustering and FCM clustering algorithms produced more fissures where the main Sulzberger glacier was melting. The PCAKM<sup>[7]</sup> algorithm has improved the crevasses in major places and enhanced the smoothness of the glacier edge. The result of PCANet<sup>[2]</sup> still has some deficiencies compared with the reference figure.

Table 1. Metrics of Bern dataset.

Method	FP	FN	OE	PCC	Kappa
K-means	360	326	686	99.24	70.35
FCM	162	554	716	99.21	62.29
PCAKM	179	150	329	99.64	85.75
PCANet	434	31	465	99.49	75.37
FFDNet-K	94	193	287	99.68	<b>86.86</b>
FFDNet-F	83	214	297	99.67	<b>86.20</b>

Table 2. Metrics of Sulzberger dataset.

Method	FP	FN	OE	PCC	Kappa
K-means	1411	610	2021	96.92	90.31
FCM	1376	624	2000	96.95	90.40
PCAKM	1111	768	1879	97.13	90.87
PCANet	473	739	1212	98.15	94.04
FFDNet-K	270	837	1107	98.31	<b>94.47</b>
FFDNet-F	1038	246	1284	98.04	<b>93.84</b>

The Kappa coefficient of PCANet on Bern dataset is 5.02 and 13.08 higher than that of K-means clustering and FCM clustering algorithm, respectively, but the detection accuracy is slightly improved

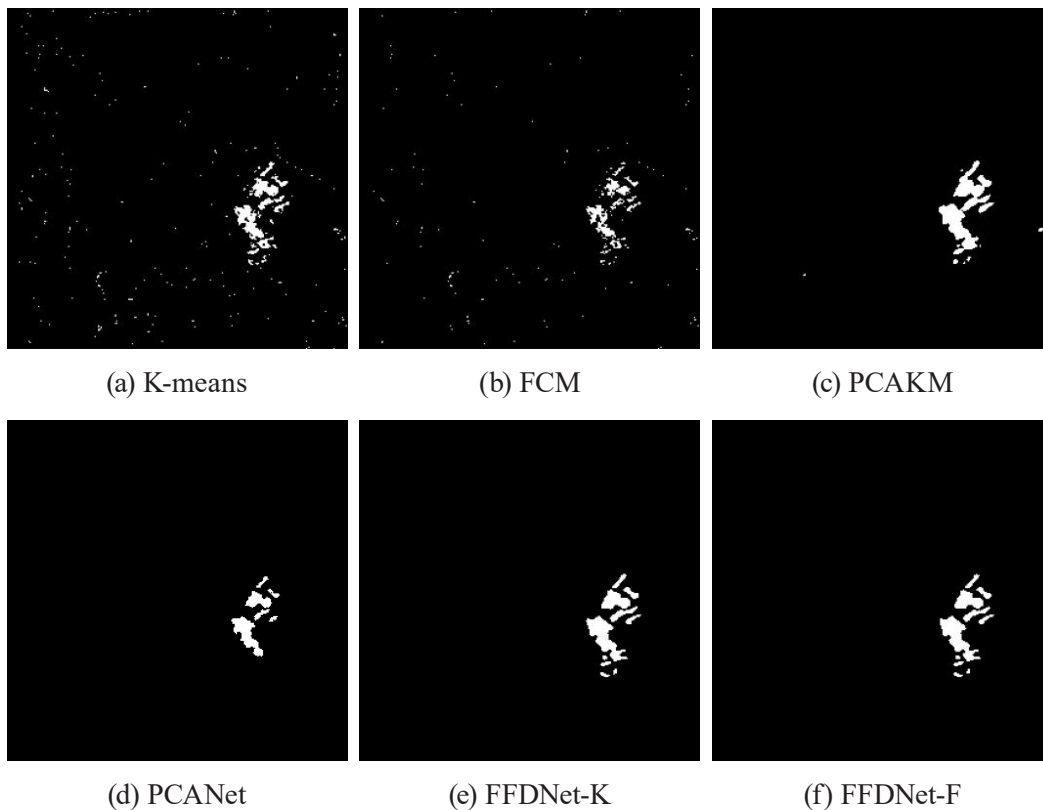


Figure 9. Change detection maps were obtained by using different methods for multi-temporal images in Bern.

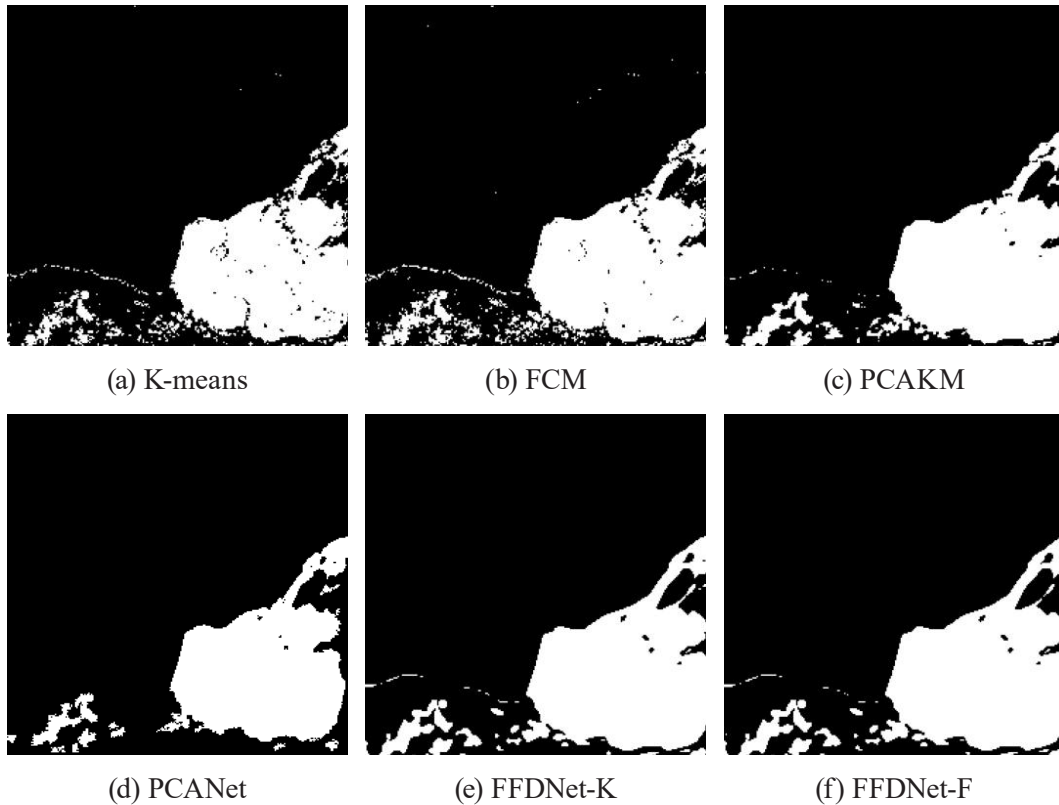


Figure 10. Change detection maps were obtained by using different methods for multi-temporal images in Sulzberger.

compared with the improved K-means clustering, that is, PCAKM algorithm. In Sulzberger dataset, it is 3.73 and 3.64 higher than K-means clustering and FCM clustering algorithm, respectively, and 3.17 higher than PCAKM algorithm. The experimental results show that the robustness to speckle noise can be improved by using PCANet algorithm, but there will be significant differences in different actual situations, and the actual content of the changing subject will be compressed in different degrees. The value of K-means and FCM after combining FFDNet in the OE index decreased significantly, and the content of the change detection results was complete, with good results in denoising and detail retention. Meanwhile, the robustness of the clustering algorithm to the noise in the difference map was improved. The Kappa coefficient of the improved results is significantly increased, indicating that the proposed method is superior to other methods.

### 3.4 Difference operator and result analysis

Different difference operators have a medium to significant impact on the final change detection results <sup>[1]</sup>, and the logarithmic ratio operator is used for subsequent classification in the experiment in Section 3.2. In order to verify the effectiveness of the method in this paper on other difference operators, the logarithmic ratio <sup>[31]</sup> and mean ratio <sup>[32]</sup> operators are compared in the clustering method, and the experimental results are shown in **Tables 3 and 4**. There are certain differences in the experimental results of the datasets using different difference operators. The overall results of the mean ratio operator in the two real datasets are lower than the logarithmic ratio. After the introduction of FFDNet spatial denoising, the Kappa coefficient is improved, and the maximum increase is 35.84 in the K-means method in the Bern dataset; the overall increase is 2.00 in the PCNet network. After the FFDNet is used to preprocess the

input original image in the spatial domain, the method in this paper is helpful in improving the Kappa coefficient in the two classical difference operators.

**Table 3.** Kappa coefficient of the Bern dataset in the mean-ratio.

<b>Kappa</b>	<b>Non-FFDNet</b>	<b>FFDNet</b>
K-means	23.30	59.14
FCM	5.90	17.58
PCAKM	37.88	58.45
PCANet	2.00	4.00

**Table 4.** Kappa coefficient of the Sulzberger dataset in the mean-ratio.

<b>Kappa</b>	<b>Non-FFDNet</b>	<b>FFDNet</b>
K-means	83.87	84.03
FCM	82.34	84.30
PCAKM	90.85	91.56
PCANet	8.00	10.00

## 4. Discussion

The method of SAR change detection allows for the quick identification and analysis of potential pollutants or abnormal conditions in water bodies by comparing image data at different time points. This approach facilitates prompt intervention by relevant authorities to ensure the safety of water sources, while also providing a scientific basis for environmental management and governance. Moreover, this technique can monitor real-time variations in parameters such as liquid level, flooding status, and soil moisture content within aquatic regions like lakes and rivers. Such information is particularly vital for the efficient allocation and administration of water resources, especially during emergency response efforts or disaster relief operations. Hence, we have chosen the widely-utilized Bern dataset as the focus of our research in this study.

The high mountain cryosphere is an extremely vulnerable and sensitive ecosystem on Earth, which has significant implications for global climate change<sup>[33]</sup>. To gain a comprehensive understanding and effectively monitor changes in this region, it is

essential to utilize appropriate technological tools. Synthetic Aperture Radar (SAR) technology utilizes electromagnetic wave reflections to provide extensive and continuously updated data of high quality. This technology plays a crucial role in studying the high mountain cryosphere. Additionally, researchers can investigate the impact of climate change on this ecosystem by analyzing long-term trends in snow coverage using historical records of multi-temporal satellite imagery. Therefore, we have chosen representative Sulzberger ice sheet data for our research paper to conduct change detection experiments and validate our analyses.

The present study emphasizes the optimization of two pivotal factors: the construction of disparity images and the clustering methodology. Through meticulous construction of disparity images coupled with the implementation of an efficient clustering technique, it becomes feasible to attain enhanced detection accuracy in change detection, particularly for real synthetic aperture radar (SAR) imagery significantly impacted by speckle noise. In order to evaluate the effectiveness of the suggested methodology, extensive experiments were carried out on two sets of well-known SAR images that are known for their significant interference caused by speckle noise. The results confirm that our approach successfully reduces speckle noise and outperforms existing techniques when assessed using robust metrics like the Kappa coefficient.

The utilization of SAR change detection is a significant approach with substantial benefits. It aids in enhancing our comprehension of intricate and nuanced dynamic procedures within a specific area, while also facilitating early detection and control of natural calamities. Moreover, it offers valuable resources for comprehending worldwide concerns like climate change.

## 5. Conclusions

To improve detection accuracy and effectively reduce speckle noise, a new method is proposed in this study. It involves the integration of transfer learning by incorporating the gray-level weights suggested

by the FFDNet team. The FFDNet is utilized as a denoising network to alleviate the noise present in the initial input Synthetic Aperture Radar (SAR) images. In order to enhance the model's performance, we integrate SAR graphics containing speckle noise during the retraining phase. This additional training helps fine-tune the model specifically for SAR images impacted by mild speckle noise, thereby improving its ability to handle such complex situations.

In conclusion, significant results have been achieved in processing SAR images with speckle noise by using FFDNet as a denoising network, optimizing the construction of difference images, and employing clustering methods. These research findings can not only be widely applied to change detection tasks in the field of remote sensing but also provide valuable references for other related fields.

## Author Contributions

Yuqing Wu: Formulation and evolution of overarching research goals and aims, writing the original draft.

Qing Xu: Writing, review & editing.

Zheng Zhang: Preparation, creation and presentation of the published work, specifically data presentation.

Jingzhen Ma: Formal analysis, verification whether as a part of the activity or separate.

Tianming Zhao: Acquisition of the financial support for the project leading to this publication.

Xinming Zhu: Acquisition of the financial support for the project leading to this publication.

## Conflict of Interest

There is no conflict of interest.

## References

- [1] Gong, M., Zhao, J., Liu, J., et al., 2015. Change detection in synthetic aperture radar images based on deep neural networks. *IEEE Transactions on Neural Networks and Learning Systems*. 27(1), 125-138.
- [2] Gao, F., Dong, J., Li, B., et al., 2016. Automatic change detection in synthetic aperture radar images based on PCANet. *IEEE Geoscience and Remote Sensing Letters*. 13(12), 1792-1796.
- [3] Touzi, R., 2006. Target scattering decomposition in terms of roll-invariant target parameters. *IEEE Transactions on Geoscience and Remote Sensing*. 45(1), 73-84.
- [4] Muhuri, A., Goita, K., Magagi, R., et al., 2023. Geodesic distance based scattering power decomposition for compact polarimetric SAR data. *IEEE Transactions on Geoscience and Remote Sensing*. 61, 1-12.
- [5] Liu, S., Gao, L., Lei, Y., et al., 2020. SAR speckle removal using hybrid frequency modulations. *IEEE Transactions on Geoscience and Remote Sensing*. 59(5), 3956-3966.
- [6] Gong, M., Zhou, Z., Ma, J., 2011. Change detection in synthetic aperture radar images based on image fusion and fuzzy clustering. *IEEE Transactions on Image Processing*. 21(4), 2141-2151.
- [7] Celik, T., 2009. Unsupervised change detection in satellite images using principal component analysis and k-means clustering. *IEEE Geoscience and Remote Sensing Letters*. 6(4), 772-776.
- [8] Gao, F., Wang, X., Gao, Y., et al., 2019. Sea ice change detection in SAR images based on convolutional-wavelet neural networks. *IEEE Geoscience and Remote Sensing Letters*. 16(8), 1240-1244.
- [9] Qu, X., Gao, F., Dong, J., et al., 2021. Change detection in synthetic aperture radar images using a dual-domain network. *IEEE Geoscience and Remote Sensing Letters*. 19, 1-5.
- [10] Shang, R., Xie, K., Okoth, M.A., et al. (editors), 2019. SAR image change detection based on mean shift pre-classification and fuzzy C-means. *IGARSS 2019-2019 IEEE International Geoscience and Remote Sensing Symposium*; 2019 Jul 28-Aug 2; Yokohama, Japan. New York: IEEE. p. 2358-2361.

- [11] Ghosh, A., Mishra, N.S., Ghosh, S., 2011. Fuzzy clustering algorithms for unsupervised change detection in remote sensing images. *Information Sciences*. 181(4), 699-715.
- [12] Zheng, Y., Zhang, X., Hou, B., et al., 2013. Using combined difference image and  $k$ -means clustering for SAR image change detection. *IEEE Geoscience and Remote Sensing Letters*. 11(3), 691-695.
- [13] Tan, S., Zhang, X., Wang, H., et al., 2021. A CNN-based self-supervised synthetic aperture radar image denoising approach. *IEEE Transactions on Geoscience and Remote Sensing*. 60, 1-15.
- [14] Zhang, K., Zuo, W., Zhang, L., 2018. FFDNet: Toward a fast and flexible solution for CNN-based image denoising. *IEEE Transactions on Image Processing*. 27(9), 4608-4622.
- [15] Hao, F., Tang, C., Xu, M., et al., 2019. Batch denoising of ESPI fringe patterns based on convolutional neural network. *Applied Optics*. 58(13), 3338-3346.
- [16] Guo, S., Yan, Z., Zhang, K., et al. (editors), 2019. Toward convolutional blind denoising of real photographs. *Proceedings of the IEEE/CVF Conference on Computer Vision and Pattern Recognition*; 2019 Jun 15-20; Long Beach, CA, USA. New York: IEEE. p. 1712-1722.
- [17] Meester, M.J., Baslamisli, A.S., 2022. SAR image edge detection: Review and benchmark experiments. *International Journal of Remote Sensing*. 43(14), 5372-5438.
- [18] De Borba, A.A., Muhuri, A., Marengoni, M., et al., 2023. Feature Selection for edge detection in PolSAR images. *Remote Sensing*. 15(9), 2479.
- [19] Mildenhall, B., Barron, J.T., Chen, J., et al. (editors), 2018. Burst denoising with kernel prediction networks. *Proceedings of the IEEE Conference on Computer Vision and Pattern Recognition*; 2018 Jun 18-23; Salt Lake City, UT, USA. New York: IEEE. p. 2502-2510.
- [20] Chierchia, G., Cozzolino, D., Poggi, G., et al. (editors), 2017. SAR image despeckling through convolutional neural networks. 2017 IEEE International Geoscience and Remote Sensing Symposium (IGARSS); 2017 Jul 23-28; Fort Worth, Texas. New York: IEEE. p. 5438-5441.
- [21] Bazi, Y., Bruzzone, L., Melgani, F., 2005. An unsupervised approach based on the generalized Gaussian model to automatic change detection in multitemporal SAR images. *IEEE Transactions on Geoscience and Remote Sensing*. 43(4), 874-887.
- [22] Rezaei, H., Karami, A. (editors), 2017. SAR image denoising using homomorphic and shearlet transforms. 2017 3rd International Conference on Pattern Recognition and Image Analysis (IPRIA); 2017 Apr 19-20; Shahrekord, Iran. New York: IEEE. p. 80-83.
- [23] Patra, S., Ghosh, S., Ghosh, A., 2011. Histogram thresholding for unsupervised change detection of remote sensing images. *International Journal of Remote Sensing*. 32(21), 6071-6089.
- [24] Mishra, N.S., Ghosh, S., Ghosh, A., 2012. Fuzzy clustering algorithms incorporating local information for change detection in remotely sensed images. *Applied Soft Computing*. 12(8), 2683-2692.
- [25] Yetgin, Z., 2011. Unsupervised change detection of satellite images using local gradual descent. *IEEE Transactions on Geoscience and Remote Sensing*. 50(5), 1919-1929.
- [26] Ghosh, S., Mishra, N.S., Ghosh, A. (editors), 2009. Unsupervised change detection of remotely sensed images using fuzzy clustering. 2009 Seventh International Conference on Advances in Pattern Recognition; 2009 Feb 4-6; Kolkata, India. New York: IEEE. p. 385-388.
- [27] Gosain, A., Dahiya, S., 2016. Performance analysis of various fuzzy clustering algorithms: A review. *Procedia Computer Science*. 79, 100-111.
- [28] Pal, N.R., Bezdek, J.C., 1995. On cluster validity for the fuzzy c-means model. *IEEE Transactions on Fuzzy Systems*. 3(3), 370-379.
- [29] Wang, Z., Bovik, A.C., Sheikh, H.R., et al., 2004. Image quality assessment: From error vis-

- ibility to structural similarity. *IEEE Transactions on Image Processing*. 13(4), 600-612.
- [30] Rosin, P.L., Ioannidis, E., 2003. Evaluation of global image thresholding for change detection. *Pattern Recognition Letters*. 24(14), 2345-2356.
- [31] Bovolo, F., Bruzzone, L., 2005. A detail-preserving scale-driven approach to change detection in multitemporal SAR images. *IEEE Transactions on Geoscience and Remote Sensing*. 43(12), 2963-2972.
- [32] Inglada, J., Mercier, G., 2007. A new statistical similarity measure for change detection in multitemporal SAR images and its extension to multiscale change analysis. *IEEE Transactions on Geoscience and Remote Sensing*. 45(5), 1432-1445.
- [33] Shugar, D.H., Jacquemart, M., Shean, D., et al., 2021. A massive rock and ice avalanche caused the 2021 disaster at Chamoli, Indian Himalaya. *Science*. 373(6552), 300-306.